Accepted Manuscript

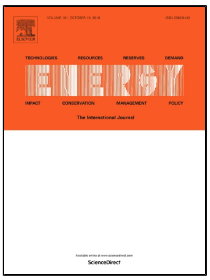

Lithium-Ion Battery Modeling and Parameter Identification Based on Fractional Theory

Minghui Hu, Yunxiao Li, Shuxian Li, Chunyun Fu, Datong Qin, Zonghua Li

PII:	S0360-5442(18)31865-6
DOI:	10.1016/j.energy.2018.09.101
Reference:	EGY 13795
To appear in:	*Energy*
Received Date:	03 May 2018
Accepted Date:	15 September 2018

Please cite this article as: Minghui Hu, Yunxiao Li, Shuxian Li, Chunyun Fu, Datong Qin, Zonghua Li, Lithium-Ion Battery Modeling and Parameter Identification Based on Fractional Theory, *Energy* (2018), doi: 10.1016/j.energy.2018.09.101

Lithium-Ion Battery Modeling and Parameter Identification Based on Fractional Theory

Minghui Hu Yunxiao Li Shuxian Li Chunyun Fu Datong Qin
State Key Laboratory of Mechanical Transmissions, School of Automotive Engineering, Chongqing University, Chongqing 400044, China
Zonghua Li
Changan New Energy Automobile Research Institute, Chongqing 401120, China

Hilghts:

A fractional-order equivalent circuit model of lithium-ion battery is established.
A MCPSO based parameter identification is conducted.
The model accuracy and robustness are verified by experiments.
The accuracy of proposed SOC estimator is discussed.

Abstract: To effectively use and manage lithium-ion batteries and accurately estimate battery states such as state of charge and state of health, battery models with good robustness, accuracy and low-complexity need to be established. So the models can be embedded in microprocessors and provide accurate results in real-time. Firstly, this paper analyzes the electrochemical impedance spectrogram of lithium-ion battery, and adopts impedance elements with fractional order characteristics such as constant phase element and Warburg element to improve the second-order RC integer equivalent circuit model based on the fractional calculus theory. Secondly, a fractional-order equivalent circuit model of lithium-ion battery is established, which can accurately describe the electrochemical processes such as charge transfer reaction, double-layer effect, mass transfer and diffusion of lithium-ion battery. Thirdly, based on the mixed-swarm-based cooperative particle swarm optimization, parameter identification of the fractional-order equivalent circuit model is conducted using the federal city driving schedule experimental data in the time domain. The simulation results show that the model has higher accuracy and better robustness against different driving conditions, different SOC ranges and different temperatures than the second-order RC equivalent circuit model. The SOC estimation accuracy based on the fractional-order equivalent circuit model of lithium-ion battery is validated.

Key words: lithium-ion battery; fractional-order model; parameter identification; particle swarm algorithm; electric vehicle

1 Introduction

Lithium-ion batteries are widely used in pure electric vehicles and hybrid vehicles because of their high specific energy, long life, and low self-discharge rate. [1] In order to use lithium-ion batteries safely and effectively, an accurate and low-complexity model is needed to describe the dynamic and static characteristics inside the battery.[2] An accurate lithium-ion battery model not only effectively improves the accuracy of state of charge (SOC) and state of health (SOH) estimation, but also enhances the simulation effectiveness when formulating the vehicle control strategy. The

lithium-ion battery modeling plays a crucial role in the analysis and control of electric vehicle power systems. To improve the accuracy, robustness and rapidity of lithium-ion battery models, many scholars have conducted relevant research and exploration. The existing lithium-ion battery models mainly fall into three categories: electrochemical models, black box models, and equivalent circuit models.[3]

Although the electrochemical models based on nonlinear coupled partial differential equations have high precision, these models present obvious drawbacks: complex model structure, difficult parameter identification, and low operation speed. They are not suitable to be used for hybrid electric vehicles and pure electric vehicles.[4] Aiming to improve practicality, some researchers simplified the electrochemical models and proposed a series of simplified models such as the pseudo two-dimensional (P2D) model,[4a] single-particle model[5] and electrode average model.[6] Moreover, the polynomial approximation,[7] Pade approximation,[8] finite volume discretization,[9] orthogonal decomposition[10]and other methods are employed to simplify the solid-state diffusion motion of lithium-ion batteries, at a cost of lower model accuracy. D. Domenico[11] proposed the electrode average model, ignoring the distribution of solid-state lithium ion concentration along the electrode direction, and introducing the average value of solid-state lithium ion concentration related to SOC. This model is simple in form, easy to implement and faster in simulation. However, the simplification of the model leads to some information loss in the battery internal reaction process, resulting in a decrease in accuracy. Haran BS et al. [12] only considered the charge transfer process inside the lithium-ion battery, and neglected the influence of liquid-phase potential energy and liquid-phase lithium ion concentration on the battery terminal voltage. A single-particle model is then established, which is only suitable for constant current and small rate discharge conditions due to excessive assumptions and simplifications.

The black box models are established by training and learning the experimental data. There is no system state equation in the model, and the model accuracy is closely related to the training data and training methods. Therefore, the black box models require a large amount of experimental data for training and learning, and can only be applied to the original training data, as a result, its robustness is unfavorable. A black box battery model based on a neural network is established using electric vehicle simulation software ADVISOR.[13] This model is a two-layer neural network, with battery load power and SOC being the inputs, and current and voltage being the outputs. WANG et al. [14]established a nonlinear black-box battery model using the support vector regression algorithm. Their results show that the maximum relative voltage error resulting from the model on the federal city driving schedule (FUDS) test data is 3.61%.

The equivalent circuit models are widely employed in vehicle simulation, SOC and SOH estimation, and battery management systems [15] due to its simplicity. However, the integer-order equivalent circuit model cannot accurately describe the dynamic process of the battery and the number of order affects its accuracy. Specifically, the low-order integer-order equivalent circuit model cannot meet the accuracy requirements, and high-order integer-order model increases the complicity of model structure and the number of parameters to be identified, while slowing down

the running speed. Hu et al. [2]conducted a detailed comparative analysis on 12 circuit models, including the internal resistance (Rint) model of lithium battery, hysteresis model considering battery state delay, third-order RC model, low-pass filtering adaptive (ESC) model, etc. In order to reduce the battery model complexity and improve SOC estimation accuracy, Liu et al. [16] proposed a fractional-order PNGV model that takes into account the effects of battery electrode composition, microstructure porosity, and electrolyte absorption rate on battery characteristics. However, the electrochemical process of the battery is not completely considered in this model. Since the parameters of equivalent circuit models are closely related to battery operating state, the effectiveness of parameter identification is very important. As for the identification of nonlinear system parameters, the current identification methods mainly include nonlinear least squares methods, [17] neural network algorithm [18] and bionic optimization algorithms. [19] Specifically, the bionic optimization algorithms include genetic algorithms (GA), [20] particle swarm optimization (PSO), [1b] bacterial community foraging optimization algorithm (BFOA), [21] etc. Compared with GA, the PSO method presents many advantages including more efficient use of memory, fewer parameters to be adjusted, and easier implementation. The mixed-swarm-based cooperative particle swarm optimization (MCPSO) can effectively coordinate the dynamic balance between local optimization and global optimization, avoid local optimum, and converge to the optimal solution faster with better accuracy. [22]

In summary, the electrochemical model, the black box model, and the integer-order equivalent circuit models can hardly achieve model accuracy, fast response, and robustness in battery SOC and SOH estimation applications. In this paper, the second-order RC integer equivalent circuit model is improved by analyzing the electrochemical impedance spectroscopy of lithium-ion batteries. Fractional-order impedance components such as constant phase element (CPE) and Walberg components are used to accurately describe the lithium-ion battery charge transfer reactions, electron layer effects, mass transfer, diffusion and other electrochemical processes. Then, a fractional equivalent circuit model is established. The relationship between the open circuit voltage (OCV) and the SOC is established based on the experimental data, and the equation parameters are fitted using MATLAB. Next, based on the MCPSO algorithm, parameters of the fraction equivalent circuit model are identified using the experimental data of the lithium-ion battery FUDS operating conditions in the time domain. Finally, the accuracy and robustness of the model are verified under different operating conditions, different SOC ranges and different temperatures. The accuracy of the model is compared with that of the second-order RC equivalent circuit model. And the accuracy of SOC estimation based on the model is compared with that based on the second-order RC equivalent circuit model.

2 Fractional order algorithm

In 1695, the German mathematician Leibnitz first proposed a fractional calculus algorithm that can handle arbitrary derivatives and integrals. [23] However, in the following 20 years, the fractional calculus algorithm had not attracted enough attention and had developed slowly. Until recently, along with the rapid development of science and technology, researchers have discovered

that the phenomena like damping, friction, mechanical vibration, dynamic rebound, and acoustic diffusion have fractional properties. Fractional order algorithms can well describe the physical characteristics of these phenomena. Nowadays, fractional-order algorithms have been widely employed in modeling and sate estimation, such as biomaterials, network traffic, robotics, viscoelastic dynamics, electrochemistry, electromagnetic fields, and permanent magnet synchronous motors. In summary, the fractional order algorithms are suitable for simulating physical systems including mass transfer, diffusion dynamics and memory hysteresis. [24] Therefore, the fractional order algorithms can be applied to describe the main electrochemical characteristics in Li-ion batteries such as solid-state diffusion and double layer effect. The commonly used mathematical symbol ${}_{t_0}D_t^{\lambda}$ in the fractional-order algorithms means that time t is integrated or differentiated in any order λ, as shown in equation (1):

$$ {}_{t_0}D_t^{\lambda} = \begin{cases} \dfrac{d^{\lambda}}{dt^{\lambda}} & \lambda > 0 \\ 1 & \lambda = 0 \\ \int_0^{\tau} (d\tau)^{-\lambda} & \lambda < 0 \end{cases} \tag{1} $$

where the real number λ represents the order, and t and t_0 are the upper and lower bounds of the operator. When $\lambda > 0$, ${}_{t_0}D_t^{\lambda}$ represents a fractional differential; when $\lambda < 0$, ${}_{t_0}D_t^{\lambda}$ represents a fractional integral; when $\lambda = 0$, ${}_{t_0}D_t^{\lambda} = 1$.

Fractional order algorithms often contain Gamma functions, which are defined as follows:

$$ \Gamma(x) = \int_0^{\infty} t^{x-1} e^{-t} dt \tag{2} $$

Among many definitions of fractional-order algorithms, three of them are commonly used. They are Caputo definition, Riemann-Liouville definition and Grunwald-Letnikov definition. [24c] In terms of control and signal processing, Grunwald-Letnikov's direct definition of discrete continuous fractional equations is straightforward, and is the easiest definition to be used in digital signal control modeling. In this paper, the initial time t_0 is 0 by default, the Grunwald-Letnikov's discrete continuous fractional equations is defined as (3):

$$ D_t^{\lambda} f(t) = \lim_{h \to 0} \frac{1}{h^{\lambda}} \sum_{i=0}^{[t/h]} (-1)^i \binom{\lambda}{i} f(t - ih) \tag{3} $$

where: h is the sampling period, $[t/h]$ is the integer part of t/h, $\binom{\lambda}{i}$ is the quadratic coefficient of Newton, $\binom{\lambda}{i}$ is shown in equation (4):

$$ \binom{\lambda}{i} = \frac{\lambda!}{i!(\lambda - i)!} = \frac{\Gamma(\lambda + 1)}{\Gamma(i + 1)\Gamma(\lambda - i + 1)} \tag{4} $$

Similar to the dynamic system of the integer-order integral equation, the fractional order system can be defined as follows:

$$a_n D^{\alpha_n} y(t) + a_{n-1} D^{\alpha_{n-1}} y(t) + \cdots + a_0 D^{\alpha_0} y(t) = \\ \mathrm{b}_m D^{\beta_m} x(t) + \mathrm{b}_{m-1} D^{\beta_{m-1}} x(t) + \cdots + \mathrm{b}_0 D^{\beta_0} x(t) \tag{5}$$

where $y(t)$ is system output, and $\mathrm{x}(t)$ denotes the system input.

Applying Laplace transform, the transfer function form equation (5) is expressed by equation (6):

$$\frac{Y(\mathrm{s})}{X(\mathrm{s})} = \frac{\sum_{j=0}^{m} b_j s^{\beta_j}}{\sum_{i=0}^{n} a_i s^{\alpha_i}} \tag{6}$$

3 Lithium-ion battery fractional model

The integer-order model cannot accurately describe the diffusion of lithium ion in the solid phase and the electric double layer electrochemical process of lithium-ion battery. In comparison, the fractional model can accurately describe the charge transfer reaction, double layer effect, mass transfer, diffusion and other electrochemical processes of lithium-ion battery, by means of fractional impedance components (such as CPE, and Walberg components).

3.1 Lithium-ion battery electrochemical impedance spectrogram analysis

Electrochemical impedance spectroscopy is an important approach to investigate the electrochemical properties of the battery. In the electrochemical impedance spectroscopy test, sinusoidal alternating current signals of different frequencies and amplitudes are applied to the battery electrochemical system, and frequency domain signal feedback is obtained. The electrochemical impedance spectrogram provides accurate impedance values at different frequencies, and the electrochemical impedance spectroscopy test can accurately reflect the dynamic response of the battery. A common lithium ion electrochemical impedance spectrogram is shown in Fig. 1, which usually can describe the dynamic characteristics of batteries. It can reflect the dynamic response of the battery except at very low operating temperatures (e.g. -30 °C). [25]This figure can be divided into three parts: [26] (1) High-frequency region of inductance effect; (2) Semi-oval mid-frequency region; (3) Straight-line low-frequency region. In the equivalent circuit models, the second-order RC model (as shown in Fig. 2) is often used to simulate the electrochemical dynamics inside the lithium-ion battery, due to its simple structure and easily identifiable parameters. The parallel RC circuits simulate the middle frequency region of the impedance spectrogram. But the solid-state diffusion of the lithium-ion battery is neglected, and the ideal capacitor cannot accurately simulate the double-layer effect. [27] The low-frequency region of the impedance spectroscopy does not have any electronic components. Therefore, the second-order RC equivalent circuit cannot completely reflect the electrochemical process，and a multiple-order RC equivalent circuit is needed to improve the model accuracy. However, a multiple-order equivalent circuit can result in high complexity, difficult parameter identification, and long simulation time.

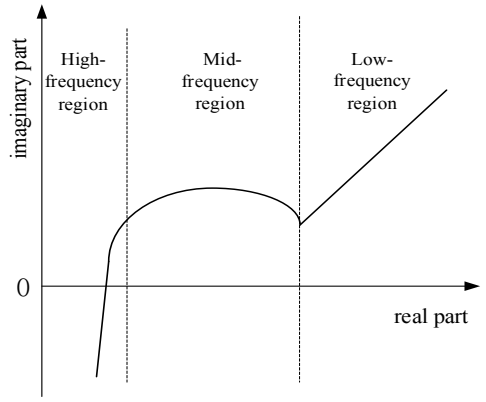

Fig 1 Impedance spectra of the Li-ion battery

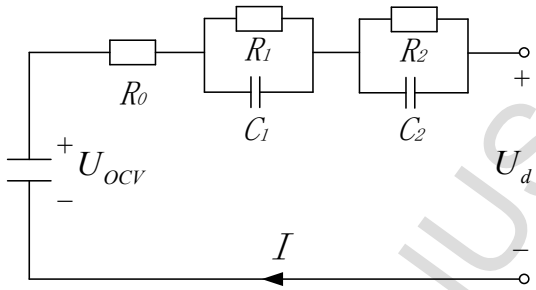

Fig 2 Structure of the 2-RC model

Therefore, based on the electrochemical process described by the electrochemical impedance spectroscopy of lithium-ion batteries, a fractional-order impedance element is introduced to improve the accuracy of the 2-RC integer-order model.

The tail of the inductive effect in the high-frequency region is caused by mass transfer, such as the transport of lithium-ions through electrolyte and porous membrane, the electron movements through wires and the transport of active material particles. The impedance spectrum curve intersects with the real axis, and the intersection point is the ohmic resistance R_0.

The half-ellipse in the middle frequency region is caused by the charge transfer reaction and the double electric layer effect, which is a common electrochemical phenomenon. It can usually be represented by a resistor in parallel with a CPE or a Volberg element. Since polarization is mainly classified into concentration polarization and electrochemical polarization, the second-order resistance is used in parallel with CPE [28] to improve the model accuracy.

The straight line in the low frequency region is caused by the solid-negative solid-phase diffusion. The straight line has a constant slope. And the low frequency region has the same characteristics of the impedance spectrum. It is usually represented by a CPE or a Volberg element. In this paper, the Volberg element representation is used.

Based on the above analysis, the fractional equivalent circuit model is drawn in Fig. 3. In this figure, U_{OCV} indicates the OCV, U_d denotes the battery terminal voltage that can be directly measured, and I represents the current (positive for charging and negative for discharging). The comparison between the 2-RC integer order model and the fractional order model is shown in Table 1.

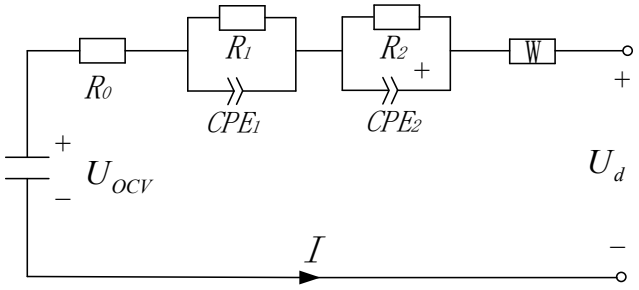

Fig 3 Schematic of the fractional equivalent circuit model

Table 1 The comparison between the 2-RC integer order model and the fractional order model

Model	2-RC equivalent circuit model	Fractional equivalent circuit model
Mid-frequency region of electrochemical impedance spectrogram	Employ the parallel RC circuits to simulate the middle frequency region But the solid-state diffusion of the lithium-ion battery is neglected, and the ideal capacitor cannot accurately simulate the double-layer effect	Using constant-phase elements with fractional order properties in parallel with resistance to accurately represent the electrochemical process of solid-state diffusion and double-layer effects of lithium-ion batteries
Low-frequency region of electrochemical impedance spectrogram	Neglect	In this paper，the Warburg element representation is used.
The number of order	Cannot completely reflect the electrochemical process，and a multiple-order RC equivalent circuit is needed to improve the model accuracy. However, a multiple-order equivalent circuit can result in high complexity, difficult parameter identification, and long simulation time.	Because the electrochemical process simulation is more complete, the accuracy of the model can be improved by using only the second-order RC fractional model, and the accuracy can be improved based on the simple model.

3.2 Establishment of Lithium-ion battery fractional model

According to the electrochemical principle, the impedance of CPE_1 in Fig. 3 is expressed in equation (7):

$$Z_{\mathrm{CPE1}} = \frac{1}{C_1 s^{\alpha}} \tag{7}$$

Then, the impedances of the CPE_2 and the Walburg element W are given by equations (8) and (9), respectively.

$$Z_{\mathrm{CPE2}} = \frac{1}{C_2 s^{\beta}} \tag{8}$$

$$Z_{\mathrm{W}} = \frac{1}{Ws^{\gamma}} \tag{9}$$

In the above equations, *C1, C2*, W are the parameters of model elements, α, β are the fractional order of CPE_1 and CPE_2 elements, and γ is the Walberg element fractional order.

Note that, CPE_1 and CPE_2 represent ideal capacitors for $\alpha=\beta=1$, and resistors for $\alpha=\beta=0$. In this paper, the lithium-ion battery is modeled based on the fractional calculus theory, and the fractional order is in the range of (0, 1). In summary, the transfer function of the fractional model impedance of lithium-ion batteries is written as:

$$\frac{U_d(s)-U_{OCV}(s)}{I(s)} = \frac{R_1}{1+R_1C_1s^{\alpha}} + \frac{R_2}{1+R_2C_2s^{\beta}} + \frac{1}{Ws^{\gamma}} + R_0 \tag{10}$$

where U_{OCV} is the OCV of lithium-ion battery, U_d is the terminal voltage of lithium-ion battery, I denotes the current of lithium-ion battery, R_0 represents the ohmic resistance of lithium-ion battery, and R_1, R_2 are the polarization resistances of lithium-ion battery.

The input to the system is set to u(t)=I(t), i.e. the battery current. The output of the system is y(t)= U_d(t)-U_{OCV}(t), namely the difference between the battery OCV and the terminal voltage. Therefore, according to equation (5), the system model uses the fractional calculus equation in the time domain as given by equation (11):

$$\begin{aligned}&(WD^{\gamma} + WR_1C_1D^{\alpha+\gamma} + WR_2C_2D^{\beta+\gamma} + \\ &WR_1C_1R_2C_2D^{\alpha+\beta+\gamma})y(t) = [R_1C_1D^{\alpha} + R_2C_2D^{\beta} \\ &+(R_0+R_1+R_2)WD^{\gamma} + R_1C_1R_2C_2D^{\alpha+\beta} + \\ &(R_0+R_2)WR_1C_1D^{\alpha+\gamma} + (R_0+R_1)WR_2C_2D^{\beta+\gamma} + \\ &R_0WR_1C_1R_2C_2D^{\alpha+\beta+\gamma}]u(\mathrm{t}) + u(\mathrm{t})\end{aligned} \tag{11}$$

By definition, the system state of the SOC as a fractional model as follows:

$$D^{1}SOC(t) = \frac{\eta}{C_{\mathrm{n}}}u(t) \tag{12}$$

where C_{n} is the battery rated capacity, η is the battery coulomb efficiency, η equals 0.98 when charging and 1 when discharging.

According to the definition in (3), the fractional derivative term contained in formula (11) is discretized as follows:

$$\begin{aligned}WD^{\gamma}y(t) &\approx \frac{W}{T^{\gamma}}\sum_{i=0}^{N}(-1)^{i}\binom{\gamma}{i}y(t-iT) \\ R_1C_1D^{\alpha}u(\mathrm{t}) &\approx \frac{R_1C_1}{T^{\alpha}}\sum_{i=0}^{N}(-1)^{i}\binom{\alpha}{i}u(t-iT)\end{aligned} \tag{13}$$

where: N is the number of historical data points involved in the calculation, and T is the sampling interval.

In this article, lumped parameters are defined as follows:

$$
\begin{aligned}
&[a_1\ \ a_2\ \ a_3\ \ a_4]=[\gamma\ \ \alpha+\gamma\ \ \beta+\gamma\ \ \alpha+\beta+\gamma]\\
&[b_1\ \ b_2\ \ b_3\ \ b_4]=[W\ \ WR_1C_1\ \ WR_2C_2\ \ WR_1C_1R_2C_2]\\
&[c_1\ \ c_2\ \ c_3\ \ c_4\ \ c_5\ \ c_6\ \ c_7]=[\alpha\ \beta\ \gamma\ \alpha+\beta\ \alpha+\gamma\ \beta+\gamma\ \alpha+\beta+\gamma]\\
&[d_1\ \ d_2\ \ d_3\ \ d_4\ \ d_5\ \ d_6\ d_7]=[R_1C_1\ \ R_2C_2\ \ (R_0+R_1+R_2)W\ \ R_1C_1R_2C_2\\
&\qquad\qquad (R_0+R_2)WR_1C_1\ \ (R_0+R_1)WR_2C_2\ \ R_0WR_1C_1R_2C_2]
\end{aligned}
\tag{14}
$$

Based on the above definition, equation (11) can be simplified as:

$$
\begin{aligned}
&\sum_{i=0}^{N}\sum_{j=1}^{4}\frac{b_j}{T^{a_j}}(-1)^i\binom{a_j}{i}y(t-iT)=\\
&\sum_{i=0}^{N}\sum_{j=1}^{7}\frac{d_j}{T^{c_j}}(-1)^i\binom{c_j}{i}u(t-iT)+u(\mathrm{t})
\end{aligned}
\tag{15}
$$

To simplify the description, define the following parameters:

$$
\begin{cases}
A(\mathrm{i})=\sum_{j=1}^{4}\frac{b_j}{T^{a_j}}(-1)^i\binom{a_j}{i}\\
B(\mathrm{i})=\sum_{j=1}^{7}\frac{d_j}{T^{c_j}}(-1)^i\binom{c_j}{i}\quad i=0,1,2\cdots N
\end{cases}
\tag{16}
$$

In the Grunwald-Letnikov definition of fractional calculus, as the sampling time T approaches 0 and N approaches infinity, the equal sign of equation (15) holds. However, in practice, as N becomes large the computation load increases. Considering the accuracy requirement of the lithium-ion battery model and the short-term memory principle, the data length can be appropriately truncated. When N=1, equation (15) can be converted to a first-order difference equation as given by:

$$
A(0)\,\mathrm{y(k)}+A(1)y(\mathrm{k}-1)=u(\mathrm{k})+B(0)u(\mathrm{k})+B(1)u(\mathrm{k}-1) \tag{17}
$$

Rearrangement of equation (17) leads to:

$$
\mathrm{y(k)}=-\frac{A(1)}{A(0)}y(\mathrm{k}-1)+\frac{1+B(0)}{A(0)}u(\mathrm{k})+\frac{B(1)}{A(0)}u(\mathrm{k}-1) \tag{18}
$$

Equation (12) can be discretized as follows:

$$
\mathrm{SOC(k)}=SOC(\mathrm{k}-1)+\frac{\eta T}{C_n}u(\mathrm{k}) \tag{19}
$$

The fractional equivalent circuit model of lithium battery is established using equations (18) and (19). This model accurately describes the lithium-ion battery dynamics with non-linear infinite order characteristics, through a simple model structure and limited number of parameters. Employing the experimental current and voltage data of the battery, the model parameters can be identified using an optimization algorithm. The parameters to be identified in the model are as follows:

$$
\theta=[\mathrm{R_0}\ \ \mathrm{R_1}\ \ \mathrm{C_1}\ \ \mathrm{R_2}\ \ \mathrm{C_2}\ \ \mathrm{W}\ \ \alpha\ \ \beta\ \ \gamma] \tag{20}
$$

4 Identification of the fractional model parameters

Before any model is successfully applied in practice, it is crucial to determine the exact value of

the parameters in the model. The battery model is complex, time-varying and nonlinearity. Besides, it involves many parameters, and some parameters cannot be directly measured. As a result, parameter identification has become a difficult problem in the battery modeling process.

4.1 Battery experiment

The schematic of the battery test system is shown in Fig. 4. This experimental equipment includes the Chongqing Weir High and Low Temperature Test Chamber (HL404C), the Ningbo Baite Battery Test Equipment (NBT530C40-T) and the host computer for human-computer interaction. According to the experimental requirements, the sampling time of the battery test system is set to 0.1s.

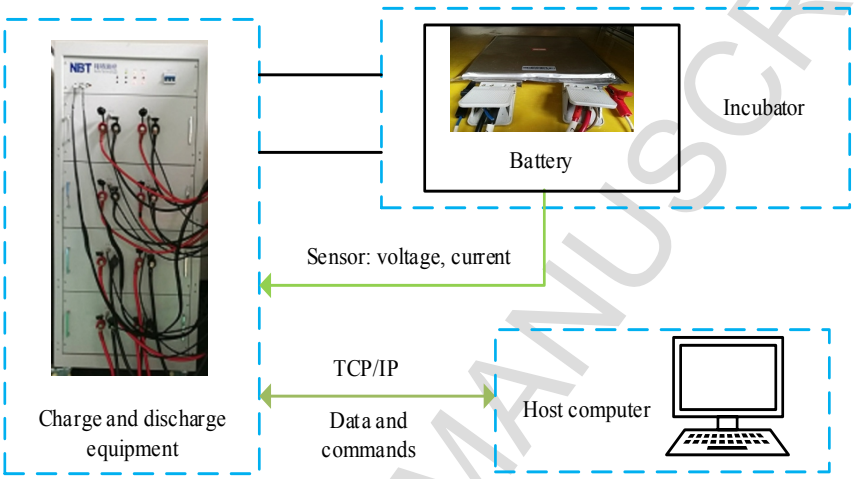

Fig 4 Schematic of the battery test system

The objects to be tested are the A123 ternary lithium ion soft pack batteries. The specifications of these batteries are shown in Table 2.

In order to identify model parameters, static capacity test (SCT), hybrid pulse power characteristic test (HPPC), FUDS condition test and dynamic stress test (DST) are performed at an ambient temperature of 25°C. The SCT test measures the available battery capacity under different discharge ratio. The HPPC test finds out the battery's power performance, open circuit voltage, DC resistance and other important features. The operating conditions of FUDS and DST are close to the actual vehicle operating conditions and can be used to identify the model parameters and verify the accuracy of the model.

Table 2 Specification of the battery

Capacity (Ah)	Charging cut-off voltage (V)	Discharge cut-off voltage (V)	Charging cut-off current (A)
25	4.2	2.5	1.25

4.2 Open circuit voltage OCV and state of charge SOC acquisition

The OCV is an important part of lithium-ion battery modeling, and it is a static characteristic parameter. Because of the polarization and hysteresis effects of lithium-ion batteries, the OCV can only be measured under sufficiently static conditions. Therefore, in an actual application, the OCV

of the battery cannot be directly measured. However, there exists a certain correspondence between the OCV and the SOC. The OCV value under a specific SOC value can be obtained through a double-pulse discharge experiment, and the relationship between the OCV and the SOC can be achieved through data fitting. The OCV values corresponding to different SOC values at 25°C is measured by the double pulse method, and the results are as shown in Table 3.

Table 3 The OCV values corresponding to different SOC values

SOC	0.1	0.2	0.3	0.4	0.5	0.6	0.7	0.8	0.9
OCV/V	3.466	3.544	3.605	3.6385	3.673	3.733	3.828	3.9205	4.0275

An empirical formula is used to fit the relationship between SOC and OCV, as given by equation (21).

$$U_{OCV}(SOC) = A_0 + A_1 SOC + A_2 \frac{1}{SOC} + A_3 \ln(SOC) + A_4 \ln(1 - SOC) \tag{21}$$

The fitted curve for the relationship between OCV and SOC is shown in Figure 5. The fitted parameters are given in Table 4.

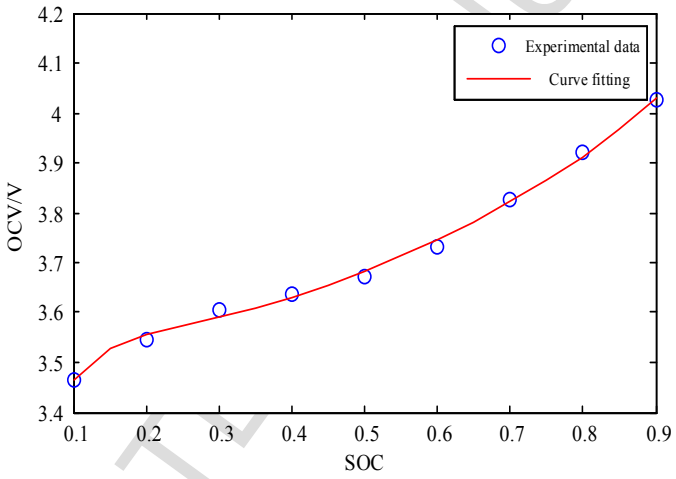

Fig 5 the fitting curve of OCV-SOC

Table 4 Fitted parameters for the OCV-SOC curve

A_0	A_1	A_2	A_3	A_4
2.9510	0.9981	-0.0515	-0.3994	-0.0856

4.3 Model parameter identification based on MCPSO algorithm

The experimental battery terminal voltage data is treated as the real value of the battery terminal voltage. The battery estimated terminal voltage is obtained using a fractional model, and the parameters in this model are identified using an optimization algorithm to minimize the error between the real and calculated/estimated terminal voltages. The objective function used for fractional model parameter identification is as follows:

$$\min_{\theta} e\left(\hat{\theta}\right) = \sum_{j=1}^{Ndata}\left[U_d(j) - \hat{U}_d(I_j, \hat{\theta})\right] \tag{22}$$

where: $e(\hat{\theta})$ is the fitness function, $\hat{\theta}$ denotes the model parameter vector to be identified, as defined in equation (20), $U_d(j)$ represents the terminal voltage data of the j-th sample point of the lithium-ion battery. Given input current I_j, and model parameter $\hat{\theta}$, the estimated voltage resulting from the fractional model output terminal is $\hat{U}_d(I_j,\hat{\theta})$.

This article uses MCPSO to carry on the parameter recognition of the above-mentioned fractional model, the concrete identification block diagram is shown in Fig. 6. MCPSO adopts the coevolutionary mechanism of two sub-populations. The entire population consists of probe sub-groups and mining sub-groups. The probe sub-group is responsible for exploring the entire solution space and performs coarse-grained search. The mining subgroup follows the probe subgroup and is responsible for the fine search in the search space of the probe subgroup so as to effectively coordinate the dynamic balance between local optimization and global optimization. The two subgroups learn from each other in the search process to realize co-evolution and converge to the optimal solution to the problem with faster efficiency and better accuracy.

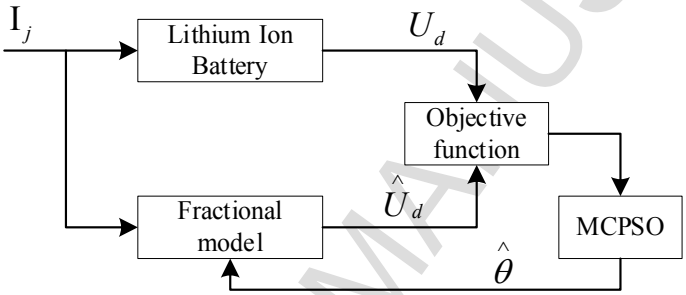

Fig 6 Structure block diagram of model parameter identification

In conjunction with this article, the model parameters to be identified are $\theta=[R_0\ R_1\ C_1\ R_2\ C_2\ W\ \alpha\ \beta\ \gamma]$, Therefore, set the particle dimension to 9, and each particle vector in the particle group is a model parameter vector. The specific optimization algorithm steps are as follows:

The steps of MCPSO-based model parameter identification are as follows:

Step 1: Mixed population initialization. Initialize the position and velocity of any particle $P_i^{S_1}$ of the test subgroup S1 in the entire solution space, and calculate the best and worst position; mining subgroup S2 is used as the subgroup of the probe subgroup, Initializes the position and velocity of any of its any particle $P_i^{S_2}$ in the active area of the test subgroup.

Step 2: Update the mixed population. The probe subgroup performs a coarse-grained search, updates the subgroups and calculates the fitness to determine the optimal and the worst locations; the mining subgroup performs a fine-grained search, updates the subgroups, and calculates the fitness to determine the optimal and the worst position.

Step 3: If the collaboration time is reached, collaborative search and learning starts among the subgroups. If the mining subgroup is superior to the probe subgroup, all particles of the probe subgroup learn from mining subgroup; if the probe subgroup is superior to the mining subgroup, all particles of the mining subgroup learn from the probe subgroup, i.e. recalculate the current

active region of the probe subgroup, and mining subgroups are regenerated in this interval.

Step 4: If the speed of the probe subgroup is less than the threshold, the mixed population performs an escape operation, i.e. resets the subgroup particle speed.

Step 5: If the termination condition is satisfied, the algorithm ends; otherwise, t = t + 1, returns to step 2.

Step 6: Output the optimal particle information for the mixed population as the optimal solution to the parameter.

The algorithm flow chart is shown in Fig. 7.

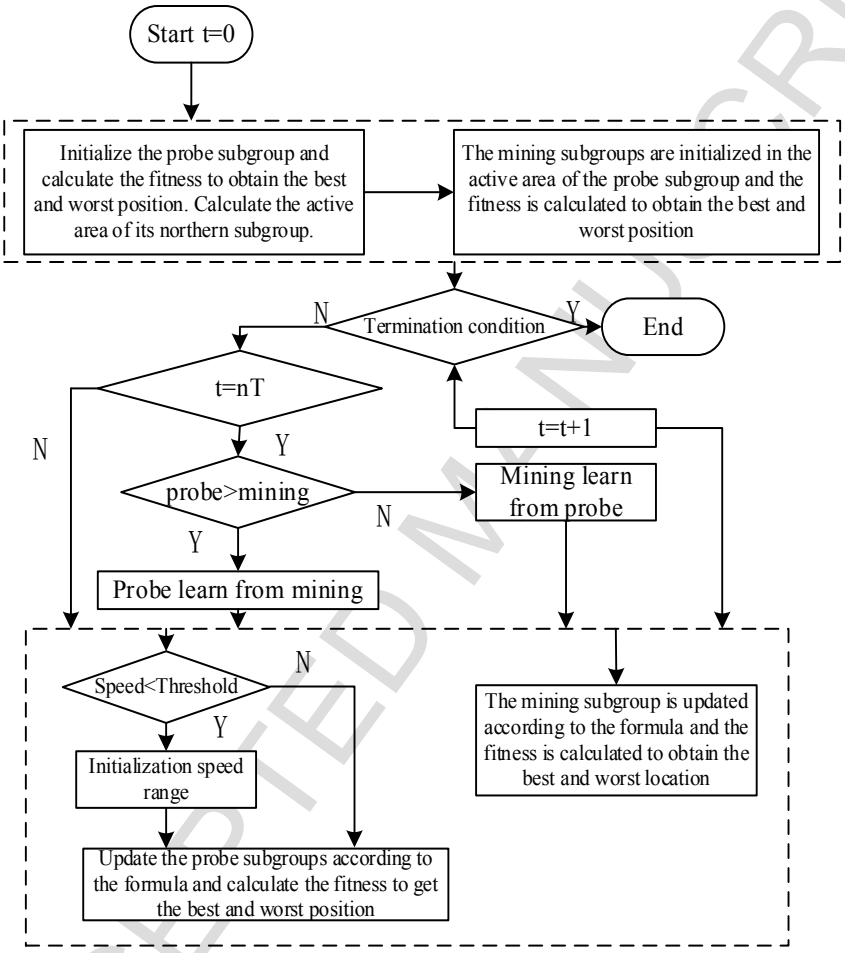

Fig 7 Flowchart for model parameter identification based on MCPSO

The algorithm parameters are shown in table 5.

Table 5 Algorithm parameter

Dimension	Size	Cooperative time	Maximum number of generations	Inertia weight	Acceleration factor
9	200	5	500	0.9-0.4	1.494

The inertia weight decreases linearly from 0.9 to 0.4, and the decline formula is as follows:

$$\omega=0.9-0.4t/\text{maxgen} \quad (23)$$

where ω denotes the inertia weight, t represents the number of current running generations, and

maxgen is the maximum number of generations.

5 Condition verification

5.1 Model parameter identification results

This paper selects the data of FUDS test cycle conditions for parameter identification of fractional equivalent paths (SOC range 0.9-0.65). The current diagram of the FUDS test cycle condition is shown in Fig. 8. The condition data is regarded as training data. The operating condition current data is used as the input of the model, and the parameters are identified based on the method of the previous section.

The parameters of the model identified using FUDS operating data are shown in Table 6.

The verification results of the fractional model on the training data are shown in Fig. 9. The error between the measured voltage and the model output voltage is shown in Fig. 10. The relative error is shown in Fig. 11. It is shown in Fig. 9 that the measured voltage is very close to the model output voltage, and the calculated root-mean-square error (RMSE) is 7.69mV. Fig. 10 shows that the absolute error is basically in the range of 20mV, and the error exceeds 20mV only when the charge-discharge current changes greatly. From Fig. 12, it is observed that the average relative error is less than 0.1%, which verifies the high accuracy of the model.

Table 6 Model parameter identification results

R_0	R_1	C_1	R_2	C_2	W	α	β	γ
0.0122	0.0084	19.7144	17.8081	51.1027	155.7854	0.8387	0.2128	0.1666

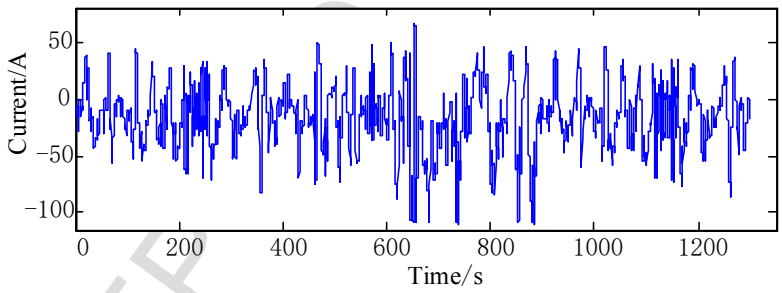

Fig 8 Current diagram of FUDS test cycle condition

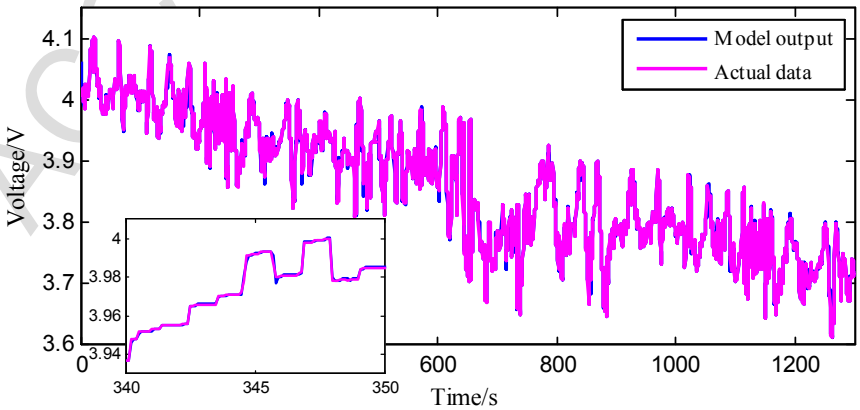

Fig 9 Comparison diagram of output voltage and measured voltage at FUDS

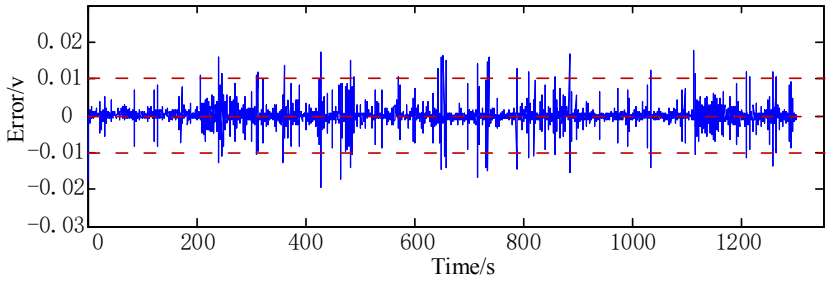

Fig 10 Error diagram of output voltage and measured voltage at FUDS

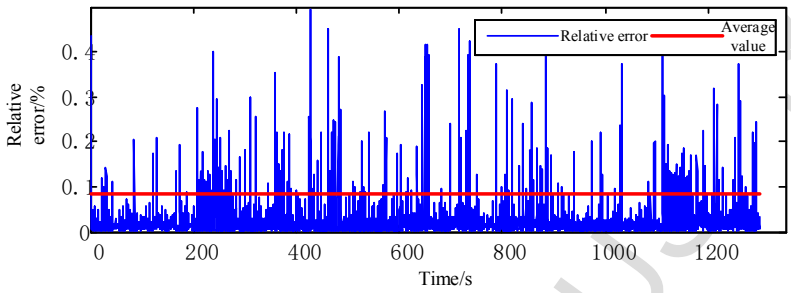

Fig 11 The relative error diagram of output voltage and measured voltage at FUDS

5.2 Verification of model robustness against different working conditions, different SOC ranges and different temperatures

When the input to the fractional equivalent circuit model is the FUDS condition cycle training data, the error between the output voltage and the measured voltage is very small, i.e. the model accuracy is very high. This section focuses on the model accuracy when non-training data is used. The non-training data mainly includes test data under different working conditions, different SOC ranges and different temperatures, which are suitable for investigating the model robustness.

The RMSE values corresponding to different operating conditions are given in Table 7. Although the frequencies of the HPPC, DST, and FUDS operating currents are different, the RMSE values under different operating conditions are still less than 10mV, which includes that the fractional-order model provides strong robustness against different working conditions.

Table 7 RMSEs for different test cycles

Operating condition	HPPC	DST	FUDS
RMSE (mV)	9.24	8.63	7.65

The RMSE values for the different SOC ranges resulting from the fractional model is shown in Table 8. It can be seen that the RMSE values are always less than 10mV in the entire SOC range. Therefore, it can be concluded that the fractional model has good robustness over the entire SOC range.

Table 8 RMSEs for different SOC ranges

SOC	0.1-0.3	0.3-0.5	0.5-0.7	0.7-0.9
RMSE (mV)	8.13	6.65	6.32	7.98

The RMSE table corresponding to fractional model at different ambient temperatures is shown in table 9. It can be seen from the table that RMSE values of models under different working conditions are still less than 15mV, and fractional order models have strong robustness at different temperatures.

Table 9 RMSEs for different temperatures

Temperature	-20℃	25℃	40℃
RMSE (mV)	14.36	6.45	9.50

5.3 Accuracy comparison of different models

To verify the advantages of fractional equivalent circuit model over the integer-order equivalent circuit model in terms of accuracy, this section compares the output voltage of the second-order RC equivalent circuit model and the fractional-order model, with step-pulse current inputs. The voltage comparison results are shown in Fig. 12, and the error comparison results are a shown in Fig. 13.

The comparative analysis of the output voltage and error in Fig. 12 and 13 reveal that the fractional model has higher accuracy. The quantitative comparison results are given in Table 10.

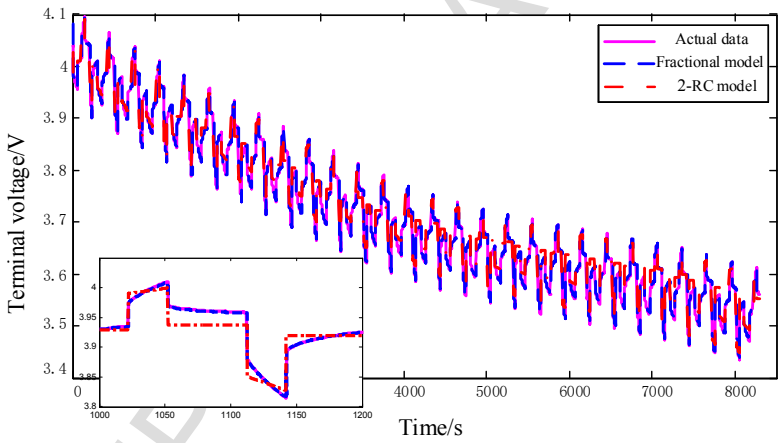

Fig 12 Output voltage comparison for different models

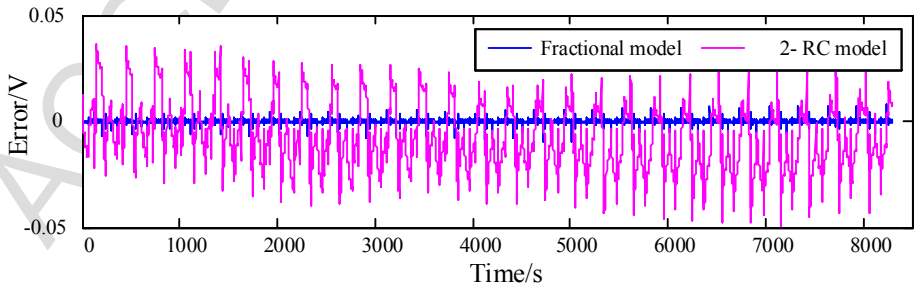

Fig 13 Output voltage errors for different models

Table 10 RMSEs and relative mean errors for different working condition and different models

	Relative Mean Error	RMSE

Second-order RC model under FUDS condition	0.396%	13.32mv
Second-order RC model under DST condition	0.395%	12.84mv
Fractional model under FUDS condition	0.085%	7.54mv
Fractional model under DST condition	0.153%	8.49mv

5.4 Accuracy comparison of SOC estimation based on different models

This section compares the SOC estimation accuracies of the extended Kalman filter, using different models - the fractional model and the 2-RC model. The initial SOC is set to the real SOC value, and the input current is under the same condition (FUDS condition). The SOC comparison results are shown in Fig. 14, and the error comparison results are shown in Fig. 15.

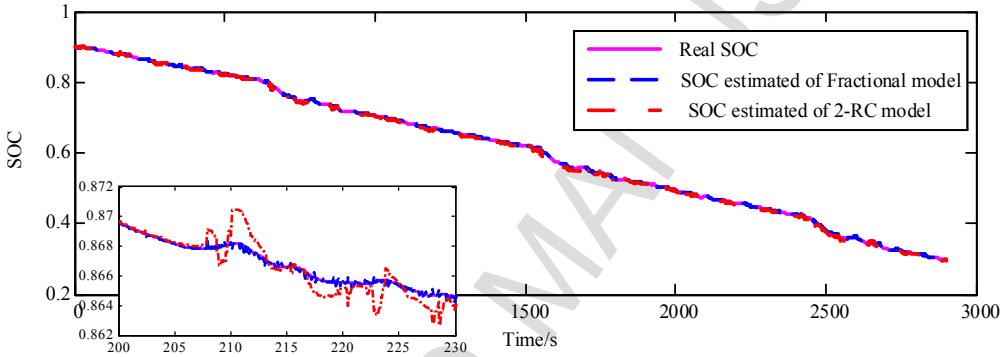

Fig. 14 SOC estimation comparison between different models

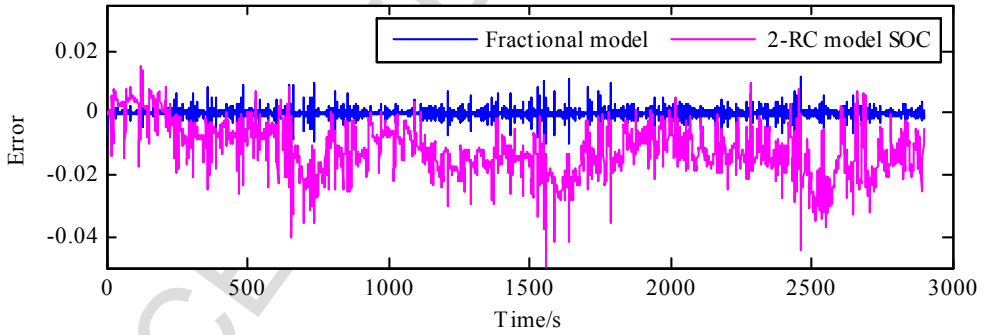

Fig. 15 SOC estimation error between different models

A comparative analysis of the results in Figs. 14 and 15 shows that the SOC estimation error based on the 2-RC model is within 0.07, while the error resulting from the fractional model is within 0.02.

The initial SOC is set to be less than the real SOC value, and the input current is under the same condition (DST condition). The SOC comparison results are shown in Fig. 16, and the error comparison results are shown in Fig. 17.

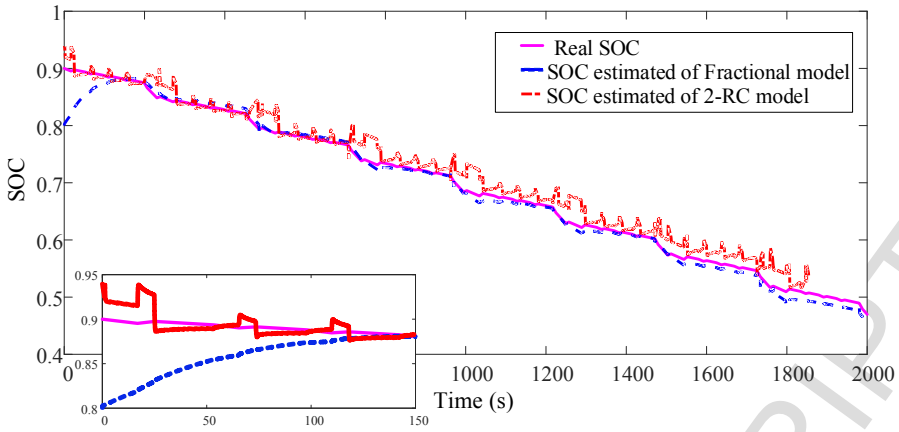

Fig 16 The SOC comparison results

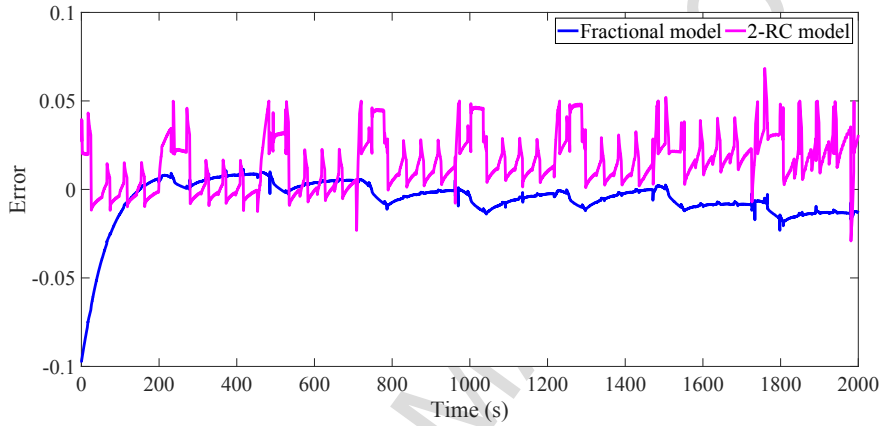

Fig 17 The SOC error comparison results

A comparative analysis of the results in Fig 16 shows that when the system has an initial error, the extended Kalman filter algorithm based on the two models can finally converge to the real SOC with a relatively small error. Although the fractional-order model converges slower comparing to the 2-RC model, it can be seen from Fig 17 that the SOC estimation error of the fractional model remains within 0.02 after the convergence is stable, and the error of the second-order RC model is within 0.07. Namely, the fractional model provides higher accuracy, which in turn proves that the model established in this paper is more accurate.

6 Conclusion

This paper based on calculus theory and the second-order RC equivalent circuit model looks into the electrochemical impedance spectroscopy of the battery, and proposes a battery equivalent circuit model using fractional components. The MCPSO algorithm is used to identify the model parameters. The RMSE of the identified model is 7.69 mV, with the absolute error, and the average relative error being less than 20 mV and 0.1% respectively. The recognition results demonstrate that the proposed fractional model has a simple structure and clear physical meaning. The parameters are easily identifiable and have high accuracy. Besides, the model accuracy and robustness are verified under different operating conditions, different SOC ranges and different temperatures. The simulation results indicate that the proposed fractional-order model presents

high accuracy not only with training data but also with different operating conditions, ~~and~~ different SOC ranges and different temperatures. This proves that the proposed model has good robustness and good applicability. Also, the accuracy of SOC estimation based on fractional-order model is validated, which indicates that this model shows obvious advantages over the second-order RC integer equivalent circuit model.

7 Funding

This work is financially supported by the National Natural Science Foundation of the People's Republic of China [No. 51675062], the National Key Research and Development Project [No. 2018YFB0106102], the Fundamental Research Funds for the Central Universities [No. 106112016CDJXZ338825], and the Major Program of Chongqing Municipality [No. cstc2015zdcy-ztzx60006].

References:

[1] aW. Su, H. Eichi, W. Zeng, M. Y. Chow, *IEEE Transactions on Industrial Informatics* **2012**, *8*, 1-10; bM. H. Amini, O. Karabasoglu, *Energies* **2017**, *11*.

[2] X. Hu, S. Li, H. Peng, *Journal of Power Sources* **2012**, *198*, 359-367.

[3] A. Seaman, T. S. Dao, J. Mcphee, *Journal of Power Sources* **2014**, *256*, 410-423.

[4] aM. Doyle, T. F. Fuller, J. S. Newman, *Journal of the Electrochemical Society* **1993**, *140*, 1526-1533; bN. Xue, W. Du, T. A. Greszler, S. Wei, J. R. R. A. Martins, *Applied Energy* **2014**, *115*, 591-602.

[5] N. Baba, H. Yoshida, M. Nagaoka, C. Okuda, S. Kawauchi, *Journal of Power Sources* **2014**, *252*, 214-228.

[6] G. Marangoni, **2010**.

[7] V. R. Subramanian, V. D. Diwakar, D. Tapriyal, *Journal of the Electrochemical Society* **2005**, *152*, A2002-A2008.

[8] J. C. Forman, S. Bashash, J. L. Stein, H. K. Fathy, J. C. Forman, S. Bashash, H. K. Fathy, *Journal of the Electrochemical Society* **2011**, *158*, A93-A101.

[9] K. Smith, C. Y. Wang, *Journal of Power Sources* **2006**, *161*, 628-639.

[10] C. Long, R. E. White, *Journal of the Electrochemical Society* **2010**, *157*, A1188-A1195.

[11] D. D. Domenico, G. Fiengo, A. Stefanopoulou, in *IEEE International Conference on Control Applications*, **2008**, pp. 702-707.

[12] B. S. Haran, B. N. Popov, R. E. White, *Journal of Power Sources* **1998**, *75*, 56-63.

[13] V. H. Johnson, *Journal of Power Sources* **2002**, *110*, 321-329.

[14] J. Wang, Q. Chen, B. Cao, *Energy Conversion & Management* **2006**, *47*, 858-864.

[15] aH. He, R. Xiong, J. Fan, *Energies* **2011**, *4*, 582-598; bW. Waag, S. Käbitz, D. U. Sauer, *Applied Energy* **2013**, *102*, 885-897.

[16] C. Liu, W. Liu, L. Wang, G. Hu, L. Ma, B. Ren, *Journal of Power Sources* **2016**, *320*, 1-12.

[17] aX. K. Chen, D. Sun, *Advances in Manu facturing* **2015**, *3*, 202-211; bS. K. Rahimian, S. Rayman, R. E. White, *Journal of Power Sources* **2011**, *196*, 8450-8462; C Y. Zhang. *On-line identification and SOC estimation of electric vehicle battery mode,* Jilin University, **2014**.

[18] Y. Y. Lin, J. Y. Chang, C. T. Lin, *IEEE Trans Neural Netw Learn Syst* **2013**, *24*, 310-321.

[19] DUAN, *Science China(Information Sciences)* **2013**, *56*, 12202-012202.

[20] J. C. Forman, S. J. Moura, J. L. Stein, H. K. Fathy, *Journal of Power Sources* **2012**, *210*, 263-275.

[21] Y. Li. *Research on the optimization algorithm of bacterial population foraging*. Harbin Institute of Technology, **2009**.

[22] J. Jie. *Intelligent particle swarm optimization*. First edition , Science Press, **2016**.

[23] C. A. Monje, Y. Q. Chen, B. M. Vinagre, D. Xue, V. Feliu, *Fractional-order Systems and Controls*, Springer London, **2010**.

[24] aC. Ma, Y. Hori, *Industrial Electronics Magazine IEEE* **2007**, *1*, 6-16; bS. Victor, R. Malti, H. Garnier, A. Oustaloup, *Automatica* **2013**, *49*, 926-935; cF. Liu, O. P. Agrawal, S. Momani, N. N. Leonenko, W. Chen, *Fractional differential equations:an introduction to fractional derivatives, fractional differential equations, to methods of their solution and some of their applications*, Academic press, **1999**.

[25] C. R. Birkl, D. A. Howey, in *Hybrid and Electric Vehicles Conference*, **2014**, pp. 2.1-2.1.

[26] S. E. Li, B. Wang, H. Peng, X. Hu, *Journal of Power Sources* **2014**, *258*, 9-18.

[27] J. B. Jorcin, M. E. Orazem, N. Pébère, B. Tribollet, *Electrochimica Acta* **2006**, *51*, 1473-1479.

[28] E. Barsoukov, J. R. Macdonald, *Impedance Spectroscopy: Theory, Experiment, and Applications, Second Edition*, Wiley-Interscience, **2005**.